Acta Crystallographica Section B
Structural Science
ISSN 0108-7681

Atomic displacements in $BiFeO_3$ as a function of temperature: neutron diffraction study

A. Palewicz,[a]* R. Przeniosło,[a] I. Sosnowska[a] and A. W. Hewat[b]

[a]Institute of Experimental Physics, Warsaw University, Hoza 69 PL 00-681, Warsaw, Poland, and [b]Institut Laue–Langevin, 6 rue Jules Horowitz, BP-156X 38 042 Grenoble, France

Correspondence e-mail: radek@fuw.edu.pl

Received 15 January 2007
Accepted 15 May 2007

The parameters of the crystal structure of $BiFeO_3$, described within the space group $R3c$, have been determined by high-resolution neutron powder diffraction for temperatures from 293 to 923 K. It was found that there is a local minimum for the rhombohedral angle α_{rh}, near the Néel temperature $T_N \simeq 640$ K, a gradual rotation of the FeO_6 octahedra and an increase of the Fe—O—Fe angle. The displacement of the Bi^{3+} ions from the FeO_6 octahedra which influence the electric polarization decreases with temperature. One of the Bi—Fe distances also has a local maximum near T_N. The atomic vibrations of Bi^{3+} and O^{2-} ions show a significant anisotropy.

1. Introduction

Recently there has been a large amount of research connected with the studies of the ferroelectric effect in multiferroic materials (Ederer & Spaldin, 2006; Fiebig, 2005; Hill, 2000). One of the most prominent examples of such materials is bismuth ferrite, $BiFeO_3$, which shows both electric polarization below $T_C = 1100$ K (Teague *et al.*, 1970) and long-range magnetic ordering below $T_N = 640$ K (Michel *et al.*, 1969). The coexistence of both electric and magnetic order parameters at room temperature is particularly interesting for technological applications. Magnetoelectric coupling is the subject of intense current research, see *e.g.* Zhao *et al.* (2006). One of the important technical applications is connected with the terahertz frequency radiation observed in $BiFeO_3$ thin films upon illumination with femtosecond laser pulses (Takahashi *et al.*, 2006); these films may be used in nonvolatile random access memories. Another important property of ceramic bulk $BiFeO_3$ is the high sensitivity to ethanol and acetone vapour, opening possibilities in semiconductor gas sensors (Poghossian *et al.*, 1991).

The magnetic ordering of $BiFeO_3$ at room temperature proposed in Sosnowska *et al.* (1982) and later confirmed in Sosnowska *et al.* (1992) and Przeniosło, Palewicz *et al.* (2006) is an antiferromagnetic ordering which is modulated with a period of 620 Å. The modulated magnetic ordering also exists above ambient temperature up to the Néel temperature of $T_N = 640$ K (Sosnowska *et al.*, 1992). The modulation of the Fe^{3+} magnetic moments in $BiFeO_3$ can be cycloidal (Sosnowska *et al.*, 1982) elliptic or even of the spin-density wave type, as discussed in Przeniosło, Regulski & Sosnowska (2006). Owing to the modulation of magnetic ordering, the linear magnetoelectric effect cannot exist in $BiFeO_3$ as was experimentally confirmed in Tabares-Muñoz *et al.* (1985), Murashov *et al.* (1991) and Kadomtseva *et al.* (2004).

Early studies of internal fields in $BiFeO_3$ studied by nuclear methods such as ^{57}Fe NMR, ^{209}Bi NMR and ^{57}Fe Mössbauer spectroscopy assumed at least two different values of the

hyperfine fields (HF) and two different quadrupole splittings (QS), see *e.g.* De Sitter *et al.* (1976). One of the early Mössbauer studies (Blaauw & Van der Woude, 1973) also suggested the possibility of a distribution of HF and QS. The existence of the modulated magnetic ordering in $BiFeO_3$ was also supported by NMR (Zalessky *et al.*, 2000; Kozheev *et al.*, 2003) and EPR (Ruette *et al.*, 2004) studies. A discussion of the modulated magnetic ordering and possible modulations of the internal fields in $BiFeO_3$ are discussed in Palewicz *et al.* (2006) and Przeniosło, Palewicz *et al.* (2006).

The values of electric polarization measured in ceramic $BiFeO_3$ are strongly sample-dependent and vary from 2.5 (Shaldin & Matyyasik, 2006) to 16.6 $\mu C\,cm^{-2}$ (Yuan *et al.*, 2006). Unusual changes of the Raman frequencies were observed in $BiFeO_3$ single crystals near $T^* = 550$ K and $T_N = 640$ K (Haumont *et al.*, 2006). Dilatometric measurements of $BiFeO_3$ show a maximum of the thermal expansion coefficient near $T_N = 640$ K (Mazumder *et al.*, 2006). A local minimum of the rhombohedral angle α_{rh} near 700 K was observed in precise $BiFeO_3$ synchrotron radiation (SR) diffraction studies (Palewicz *et al.*, 2006).

All these phenomena are related to changes of the positions of Bi^{3+}, Fe^{3+} and O^{2-} ions in the unit cell of $BiFeO_3$. Unfortunately, there are no experimental reports of direct measurements of the electric polarization of $BiFeO_3$ at temperatures above room temperature because of its low resistivity at elevated temperatures (Yuan *et al.*, 2006; Shaldin & Matyyasik, 2006). There are, however, recent studies of electric polarization in $BiFeO_3$ films at temperatures up to 800 K measured using a combination of piezoelectric force microscopy, photoemission electron microscopy and X-ray linear dichroism at a synchrotron source (Zhao *et al.*, 2006).

In order to interpret the various phenomena: *e.g.* changes in Raman spectra, anisotropic thermal expansion and the electric polarization, it is essential to have highly accurate information on the $BiFeO_3$ crystal structure under different external conditions. Our previous SR diffraction studies (Palewicz *et al.*, 2006) could not provide the relevant structural data, except for the lattice constants. Instead of the continuous Debye–Scherrer rings expected in an SR microbeam diffraction measurement with $BiFeO_3$, there are clearly separated spots, see Fig. 2 of Palewicz *et al.* (2006). It can be concluded that $BiFeO_3$ polycrystalline powder has large domains and that there is no accurate averaging of the grain orientations, as in the case with a strong texture. It is interesting to note that there are numerous X-ray diffraction studies of $BiFeO_3$ (Yuan *et al.*, 2006; Mahesh Kumar *et al.*, 2000; Pradhan *et al.*, 2005; Fruth *et al.*, 2005; Kim *et al.*, 2005; Zhang *et al.*, 2005), but in most cases without crystal structure determination. In some cases the strong texture-like effects in the X-ray diffraction patterns lead to $BiFeO_3$ structure models with unrealistic interatomic distances of nearest-neighbor Fe—O as long as 2.82 Å and nearest-neighbor Bi—O as short as 1.68 Å, as reported by Zhang *et al.* (2005).

The best method of $BiFeO_3$ crystal structure determination from polycrystalline material is neutron diffraction. Owing to the large illuminated sample volume, the texture-like effects can be correctly averaged. The good agreement with atomic position parameters of $BiFeO_3$ determined in numerous earlier neutron diffraction studies (Michel *et al.*, 1969; Fischer *et al.*, 1980; Sosnowska *et al.*, 2002) provides confidence in this method. Therefore, we performed high-resolution neutron diffraction studies of the $BiFeO_3$ polycrystalline material at temperatures above room temperature with the aim of improving the accuracy of previous studies (Fischer *et al.*, 1980).

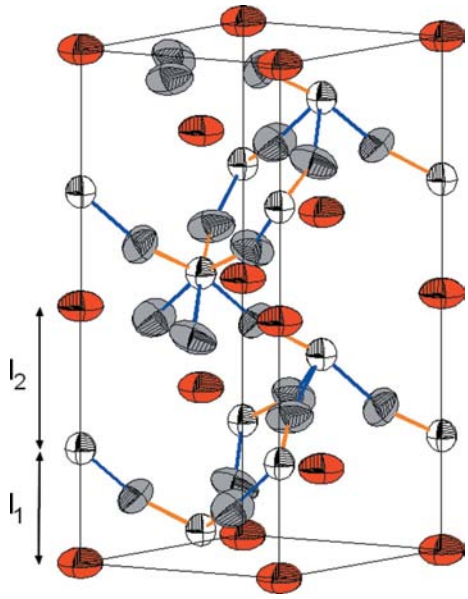

Figure 1
Schematic representation of the $BiFeO_3$ unit cell shown in the hexagonal setting of the space group *R3c*. The Bi^{3+}, Fe^{3+} and O^{2-} ions are represented by atomic displacement ellipsoids of red, white and grey, respectively. The long and short Fe—O bonds are shown in blue and orange colours, respectively. The short and long Bi—Fe distances, l_1 and l_2 (see text) are shown.

2. Experimental

The ceramic $BiFeO_3$ sample was prepared using a procedure described by Achenbach *et al.* (1967). The present studies were performed with the same polycrystalline $BiFeO_3$ sample used previously in neutron (Sosnowska *et al.*, 1992, 2002; Przeniosło, Palewicz *et al.*, 2006) and SR (Palewicz *et al.*, 2006) diffraction studies. The neutron powder diffraction measurements of $BiFeO_3$ were performed using the D2B diffractometer at ILL Grenoble, operating at a neutron wavelength of 1.5944 (1) Å. The powder $BiFeO_3$ sample was placed in an 8 mm diameter vanadium container and mounted in a furnace. The measured neutron diffraction patterns were collected for the $4 < 2\theta < 160^\circ$ range, which corresponds to the $0.3 < Q < 7.7$ $Å^{-1}$ scattering vector range, where $Q = (4\pi/\lambda)\sin\theta$ and the scattering angle is 2θ. The measurements were performed at several temperatures between room temperature and 973 K. The neutron powder diffraction patterns for $BiFeO_3$ were analyzed by the Rietveld method using the refinement

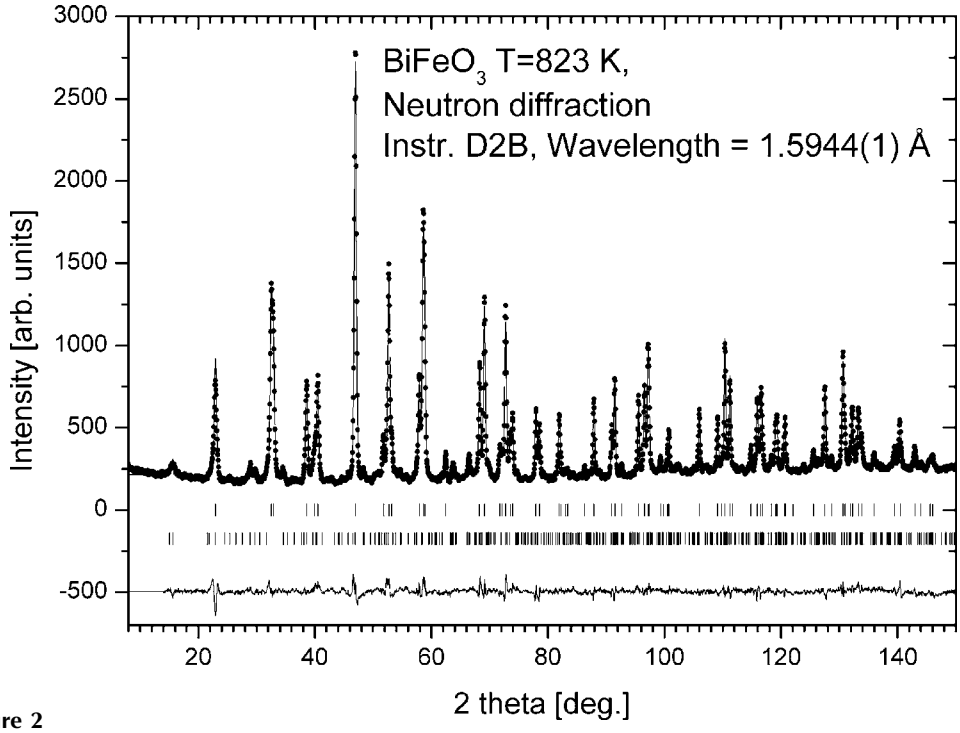

Figure 2
Results of the Rietveld refinement of the neutron powder diffraction pattern of $BiFeO_3$ measured at 823 K. The solid circles represent measured data, while the solid line represents the calculated diffraction pattern. Below the graph there is a difference curve. The ticks indicate the positions of the Bragg peaks owing to $BiFeO_3$ (Sosnowska *et al.*, 2002) and to the $Bi_2Fe_4O_{11}$ (Tutov & Markin, 1970) phases.

program *FULLPROF* (Rodríguez-Carvajal, 1993). The wavelength calibration and instrumental resolution were determined using the diffraction pattern of a reference CeO_2 sample measured in the same experimental setup.[1]

3. Results

The neutron powder diffraction pattern observed at room temperature gives Bragg peaks which agree with the $BiFeO_3$ crystal structure described by the space group *R*3*c* (Fischer *et al.*, 1980; Kubel & Schmid, 1990; Sosnowska *et al.*, 2002). The crystal structure of $BiFeO_3$ at ambient temperature (Michel *et al.*, 1969; Kubel & Schmid, 1990; Sosnowska *et al.*, 2002; Fischer *et al.*, 1980) is described in the trigonal space group *R*3*c* with the lattice parameters a = 5.58102 (4) and c = 13.8757 (4) Å, see *e.g.* Palewicz *et al.* (2006), given in the hexagonal setting which will be used in this paper. There are four positional parameters to be determined: Bi(0,0,0); Fe (0,0,z_{Fe}) and O (x_O,y_O,z_O). There are no unindexed Bragg peaks which confirms the fact that the sample is single phase, as observed in SR diffraction studies (Palewicz *et al.*, 2006). A recent review (Abrahams, 2006) of many rhombohedral compounds discusses the possibility of the incorrect description of their structures with the space group *R*3. Our $BiFeO_3$ neutron (present) and SR (Palewicz *et al.*, 2006) diffraction patterns do not show Bragg peaks that are forbidden within the *R*3c group and allowed in the *R*3 group.[2]

A schematic plot of the hexagonal unit cell of $BiFeO_3$ determined from our data at 823 K is shown in Fig. 1. The Bi^{3+} and Fe^{3+} ions are displaced with respect to each other, so there are short and long Bi—Fe distances, denoted as l_1 and l_2, respectively. Each Fe^{3+} ion has a distorted oxygen octahedron with three short (orange, $\sim$1.952 Å) and three long (blue, $\sim$2.105 Å) Fe—O bond lengths.

There are magnetic Bragg peaks due to the long-range modulated magnetic ordering of Fe^{3+} magnetic moments in $BiFeO_3$ (Sosnowska *et al.*, 1982, 1992; Przeniosło, Palewicz *et al.*, 2006). The splitting of magnetic satellite peaks seen previously in Sosnowska *et al.* (1982, 1992) and Przeniosło, Palewicz *et al.* (2006) could not be observed because of resolution limitations of the instrument at long *d* spacings with this relatively short neutron wavelength (Fig. 2).

The neutron diffraction pattern measured at the highest temperature, *i.e.* 973 K, shows the appearance of 10 new Bragg peaks. These peaks can be fully described by assuming the presence of a new phase of $Bi_2Fe_4O_9$ (Niizeki & Wachi, 1968; Tutov & Markin, 1970; Shamir *et al.*, 1978) which was created during our measurements at 973 K. Rietveld analysis shows that 11% of the sample volume was transformed to the new $Bi_2Fe_4O_9$ phase. The partially decomposed sample cooled down to room temperature also shows the same amount (11 vol.%) of $Bi_2Fe_4O_9$.

Anisotropic displacement parameters were refined for all the ions in the $BiFeO_3$ structure as already proposed in Kubel & Schmid (1990). The occupancy of the oxygen ions was also refined. The additional $Bi_2Fe_4O_9$ crystal structure was described within the orthorhombic space group *Pbam* with fixed atomic positions, as given in Tutov & Markin (1970); we refined the three lattice parameters *a*, *b* and *c* of $Bi_2Fe_4O_9$ as a function of temperature. In order to visualize the quality of

[1] Further details of the crystal structure investigations may be obtained from Fachinformationszentrum Karlsruhe, 76344 Eggenstein-Leopoldshafen, Germany (fax: +49 7247-808-666; e-mail: crysdata@fiz-karlsruhe.de, on quoting the deposition numbers from CSD-417303 to CSD-417312.

[2] Supplementary data for this paper are available from the IUCr electronic archives (Reference: CK5024). Services for accessing these data are described at the back of the journal.

data, the results of the Rietveld refinements of the neutron diffraction pattern measured at 823 K using the $BiFeO_3$ and $Bi_2Fe_4O_9$ phases are shown in Fig. 2.

The refined oxygen occupancy is *ca* 1.005 (10), so the nominal stoichiometry of $BiFeO_3$ is confirmed. The widths of the Bragg peaks for $BiFeO_3$ and CeO_2 (reference sample) are equal within statistical error. It can be concluded that the $BiFeO_3$ internal strains are negligible. The lattice parameters of $BiFeO_3$ determined from our measurements, see Fig. 3, agree with the values determined recently from high-resolution SR diffraction (Palewicz *et al.*, 2006).

The modulated magnetic ordering, described in Sosnowska *et al.* (1982), has been added to the Rietveld calculations by assuming a fixed value of the modulation length which is in agreement with earlier neutron diffraction studies (Sosnowska *et al.*, 1982, 1992; Przeniosło, Palewicz *et al.*, 2006). The value of the ordered Fe^{3+} magnetic moment refined at room temperature give $\mu_{Fe} = 3.86\,(4)\mu_B$, in agreement with previous studies (Sosnowska *et al.*, 2002).

Table 1
Agreement factor ranges for all refinements.

No. of temperatures	10
T_N (K)	640
R_p	0.0398–0.0505
R_{wp}	0.0513–0.0676
R_{exp}	0.0563–0.0566
Magnetic *R* factor	0.0538–0.0852
Bragg *R* factor	0.0303–0.0446
χ^2	0.82–1.44
Temperature range (K)	293–923

We consider the sum of the intensities of magnetic Bragg peaks located around (101) and (003) divided by the intensity of the nuclear Bragg peak (012): $R = (I_{101} + I_{003})/I_{012}$. The square-root values of *R* obtained in our present measurements are compared with the results from Haumont *et al.* (2005) in Fig. 4 (both datasets were multiplied by arbitrary scale factors in order to have equal values of *R* at 473 K). Our results agree with those from Haumont *et al.* (2005) and confirm that $T_N =$ 640 K.

The values of the lattice and positional parameters obtained from Rietveld refinements of the $BiFeO_3$ structure are shown in Table 1 of the supplementary material. The values of the anisotropic displacement factors U^{ij} are presented in Table 2 of the supplementary material and summarized in Table 1.

In order to visualize the most important structural changes we show the temperature dependence of the rhombohedral

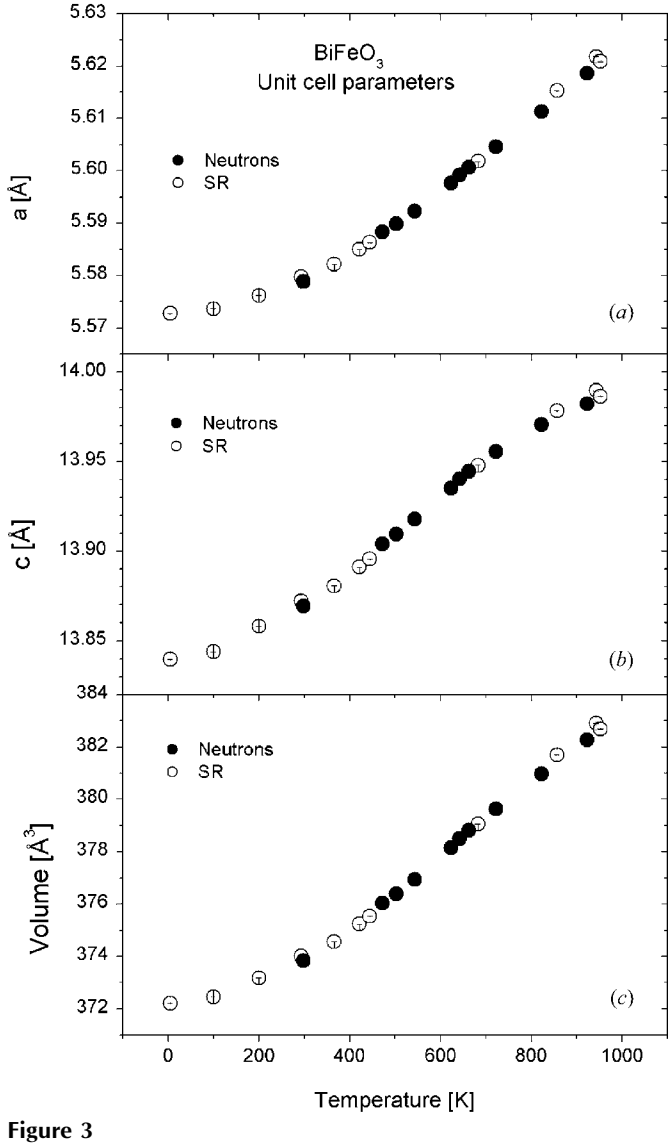

Figure 3
Temperature dependence of the $BiFeO_3$ lattice constants *a* and *c*, and the hexagonal unit-cell volume determined from the present neutron diffraction data (solid circles) and previous SR studies (empty circles; Palewicz *et al.*, 2006).

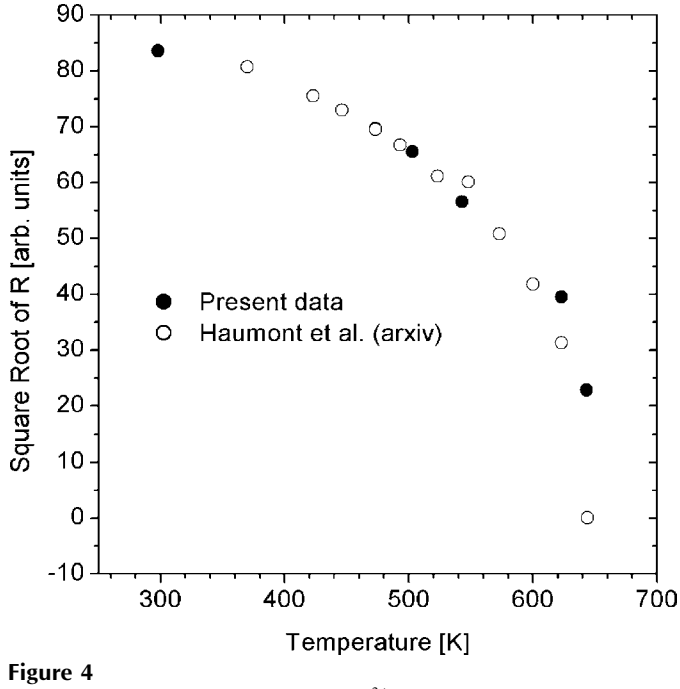

Figure 4
Temperature dependence of the Fe^{3+} normalized square root of magnetic-to-nuclear Bragg peak intensity ratio $R^{1/2}$ (see text) determined from the present neutron diffraction data (full circles) and Haumont *et al.* (2005) (open circles).

angle α_{rh} determined from the present data and SR diffraction data (Palewicz *et al.*, 2006). In Fig. 5(*a*) one can see a well pronounced minimum of α_{rh} near 750 K and an inflection point near $T^* = 550$ K. Another important feature is the monotonic increase of the z coordinates of Fe^{3+} and O^{2-} ions, as shown in Fig. 5(*b*). The FeO_6 octahedra gradually move further away from the Bi^{3+} ions located at fixed positions $z = 0$. Both short (~1.952 Å) and long (~2.105 Å) Fe—O bond lengths gradually increase with temperature (see Fig. 6).

The temperature dependence of the shorter and longer Bi—Fe distances along the c axis (denoted as l_1 and l_2) are shown in Figs. 5(*c*) and (*d*), respectively. As z_{Fe} and the lattice parameter c both increase with temperature, the shorter Bi—Fe distance $l_1 = z_{Fe}c$ also increases with temperature. The temperature changes of z_{Fe} and the c lattice parameter are such that the longer Bi—Fe distance $l_2 = (\frac{1}{2} - z_{Fe})c$ has a local maximum near $T^* = 550$ K (Fig. 5*d*). This local maximum of the long Bi—Fe distance is also confirmed by earlier neutron diffraction studies (Fischer *et al.*, 1980). Please note that the maximum of l_2 (Fig. 5*d*) and the minimum of α_{rh} (Fig. 5*a*) are not at the same temperature.

The shifts of Bi^{3+} and Fe^{3+} ions from their ideal perovskite positions contribute to spontaneous polarization. The temperature dependence of these shifts is shown in Figs. 5(*e*) and (*f*), respectively. The shift of Bi^{3+} ions gradually decreases with temperature, while the shift of Fe^{3+} ions remains constant within statistical error, 0.252 (6) Å. These values agree with earlier neutron diffraction results (Fischer *et al.*, 1980), where the shifts for Bi^{3+} and Fe^{3+} ions from their ideal perovskite positions were calculated as *sc* and *tc* (where the relative shifts t and s were defined in Megaw & Darlington, 1975, and c is the lattice parameter).

The O—Fe—O angles inside the octahedra remain constant within statistical error. There is, however, a monotonic increase of the Fe—O—Fe angle (where the two Fe^{3+} are in the centers of neighboring octahedra) from 155.3° at room temperature up to 156.8° at 923 K (see Fig. 7). There is also a monotonic decrease of the oxygen octahedra rotation angle ω (as defined in Megaw & Darlington, 1975) from 12.8° at room temperature down to 12.0° at 923 K (see Fig. 7).

Another important effect is connected with

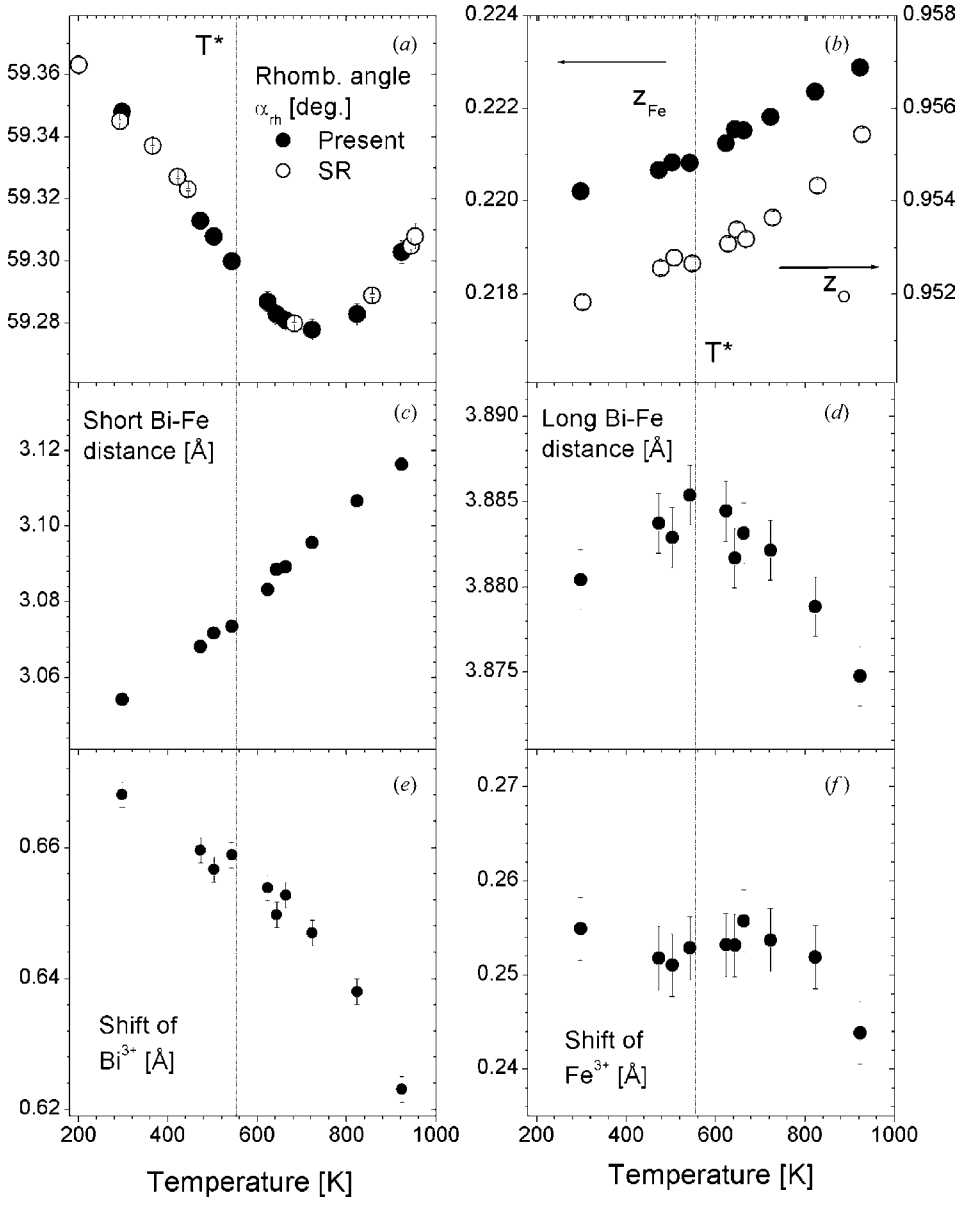

Figure 5
Temperature dependence of several structural parameters of $BiFeO_3$. The angle α_{rh} (°) is shown in (*a*), where the full and open circles show the present neutron data and previous SR diffraction data (Palewicz *et al.*, 2006), respectively. Panels (*b*)–(*f*) show the parameters determined from the present neutron diffraction data. The fractional coordinates of Fe^{3+} ions (z_{Fe} as solid circles) and O^{2-} ions (z_O as empty circles) are shown in (*b*). The short (l_1) and long (l_2) Bi—Fe distances are shown in (*c*) and (*d*), respectively. The shift of the Bi^{3+} and Fe^{3+} ions with respect to their positions in the ideal perovskite structure are shown in (*e*) and (*f*), respectively. The vertical dashed line indicates $T^* = 550$ K.

the anisotropic thermal motion of the ions. As it is difficult to separate thermal and static disorder contributions we will consider the sum of them and use the term mean-square atomic displacements (following the recommendation given in the *International Tables for Crystallography*, 2003, Vol. D, p. 228). The important anisotropies in the mean-square atomic displacements can clearly be seen in the temperature dependence of two neighbouring (220) and (208) Bragg peak intensities, as shown in Fig. 8(*a*).

The intensity of (220) decreases much faster with temperature than does (208). The amplitudes of the mean-square displacements along directions in the *ab* plane are larger than those along the *c* axis. This anisotropy was already observed in single-crystal X-ray diffraction studies of $BiFeO_3$ (Kubel & Schmid, 1990) at room temperature. The mean-square atomic displacement parameters show a nearly isotropic behaviour for Fe^{3+} ions and a strongly anisotropic behaviour for both Bi^{3+} and O^{2-} ions. This effect is seen in Fig. 1 where the root mean-square atomic displacement ellipsoids refined from $BiFeO_3$ diffraction data at 823 K are shown. One can see that the amplitude of the mean-square atomic

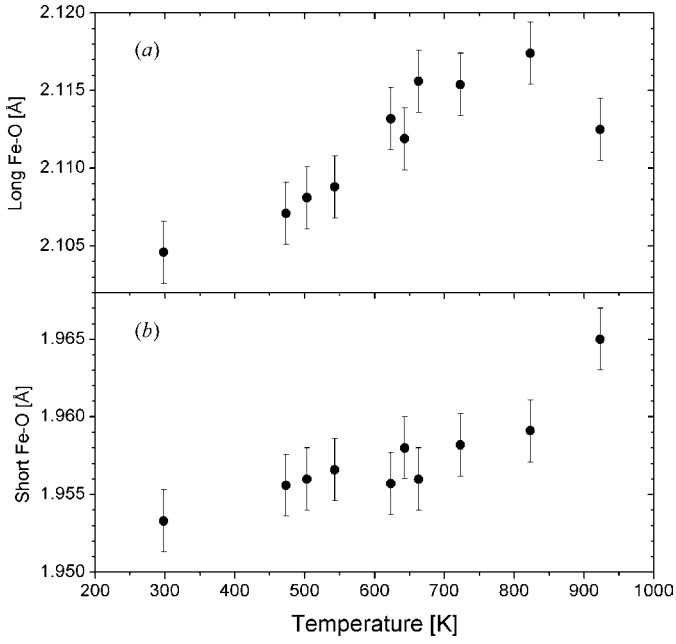

Figure 6
The temperature dependence of the shorter and longer Fe—O bond lengths (shown in orange and blue in Fig. 1, respectively) in $BiFeO_3$ determined from Rietveld analysis of neutron powder diffraction data.

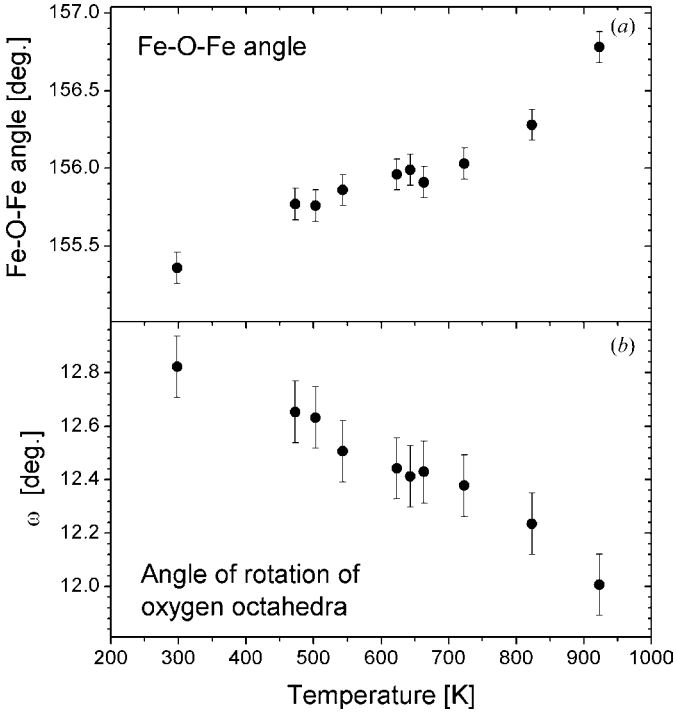

Figure 7
Values of the Fe—O—Fe angle and oxygen octahedra rotation angle ω (see Megaw & Darlington, 1975) in $BiFeO_3$ obtained from the Rietveld refinement of neutron powder diffraction patterns.

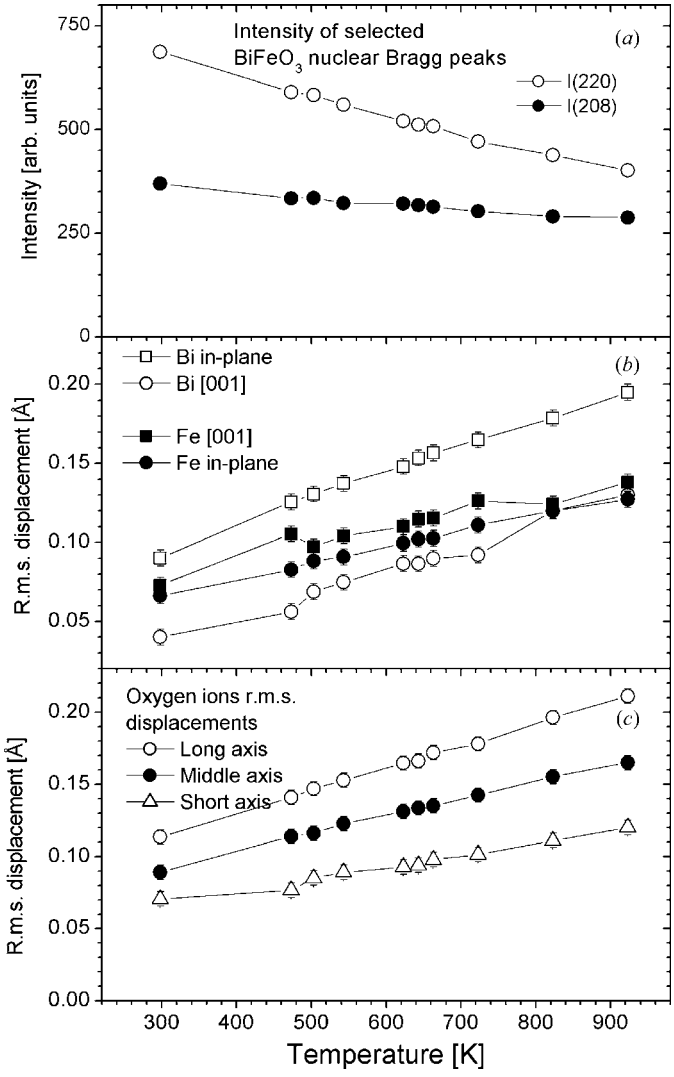

Figure 8
Temperature dependence of the intensities of the (208) and (220) nuclear Bragg peaks measured for $BiFeO_3$ with the neutron powder diffraction method (*a*). Temperature dependence of the root mean-square atomic displacements along the main axes of the displacement ellipsoids for Bi^{3+}, Fe^{3+} (*b*) and O^{2-} (*c*).

displacement of Bi^{3+} ions in the *ab* plane is approximately twice that along the *c* axis. On the other hand, the root mean-square atomic displacement ellipsoids for O^{2-} ions have three different axial lengths. The largest amplitude is in the direction perpendicular to the plane of the two Fe—O bonds. The temperature dependence of the r.m.s atomic displacements along the main axes of the displacement ellipsoids for Bi^{3+}, Fe^{3+} and O^{2-} ions are shown in Figs. 8(*b*) and (*c*).

4. Discussion

The main structural changes of $BiFeO_3$ shown in this study are the following:

(i) the FeO_6 octahedra are displaced relative to the sublattice of Bi^{3+} ions,

(ii) the FeO_6 octahedra perform a coherent rotation in which the Fe—O—Fe angles increase,

(iii) one of the Bi—Fe distances has a local maximum near $T^* = 550$ K, and

(iv) the most important contribution to the temperature changes of the electric polarization of $BiFeO_3$ comes from the shift of the Bi^{3+} ions with respect to their positions in the ideal perovskite structure.

The corresponding shift of the Fe^{3+} ions does not change with temperature. If one assumes simply a point-charge model for the calculation of the electric polarization of $BiFeO_3$, it can be expected that on warming from room temperature up to 900 K the relative polarization decrease should be of the order 6%, *i.e.* the same as the relative decrease of the shift of Bi^{3+} ions (see Fig. 5*e*).

Recent studies of the electric polarization in $BiFeO_3$ (Zhao *et al.*, 2006) reveal the existence of polarized domains with different polar axes directions. The switching between different polarization directions with the application of electric fields has been already discussed in $BiFeO_3$ single-crystal studies (Kubel & Schmid, 1990). Our present neutron diffraction data agree well with a structural model assuming only one type of polar domains.

It is important to note that the root mean-square atomic displacement ellipsoids are almost isotropic for Fe^{3+} ions and strongly anisotropic for Bi^{3+}. The mean-square atomic displacements for the Fe^{3+} ions are smaller than those of Bi^{3+}. This result holds for all temperatures and it is in agreement with the room-temperature single-crystal $BiFeO_3$ studies (Kubel & Schmid, 1990). If the masses of Bi^{3+} and Fe^{3+} ions are taken into account, the mean-square atomic displacement magnitudes should be reversed. We believe that this reversal is due to librations that resemble the situation in calcite, $CaCO_3$, at 1200 K (Dove *et al.*, 2005). In $CaCO_3$ there is a very large librational amplitude for the CO_3 groups rotating about the *c* axis, see Fig. 5 in Dove *et al.* (2005). In such a case the atomic displacement of C (lighter cation) seems small and isotropic, while Ca (heavier cation) shows a larger anisotropic displacement (Dove *et al.*, 2005). The present effects observed in $BiFeO_3$ are also similar to those reported for K_2PtCl_6 in Schefer *et al.* (1998). They introduced a libration amplitude and they calculated r.m.s. libration amplitudes of 4.3° at 380 K. We can estimate the libration amplitude in $BiFeO_3$ approximately by calculating the angles in a triangle composed of two perpendicular lengths equal to the Fe—O bond and the r.m.s. oxygen displacement. Taking the temperature dependence of the larger r.m.s. atom displacement we estimate that the libration amplitude for the Fe—O bonds changes from *ca* 3 to 5.4° for room temperature and 923 K, respectively. As can be seen in Fig. 1, there are probably librations of Fe—O bonds of different amplitude in two perpendicular directions and these librations influence the atomic displacements of Bi. A quantitative description of this phenomenon will follow.

Our present results together with the Raman studies (Haumont *et al.*, 2006) clearly show the need for further studies on various phenomena connected with the lattice dynamics of $BiFeO_3$ at high temperatures.

This work is partially supported by the Ministry of Education and Science (Poland).

References

Abrahams, S. C. (2006). *Acta Cryst.* B**62**, 26–41.

Achenbach, G. D., James, W. J. & Gerson, R. (1967). *J. Am. Ceram. Soc.* **50**, 437.

Blaauw, C. & Van der Woude, F. (1973). *J. Phys. Solid State Phys.* **6**, 1422.

De Sitter, J., Dauwe, C., De Grave, E. & Govaert, A. (1976). *Solid State Commun.* **18**, 645.

Dove, M. T., Swainson, I. P., Powell, B. M. & Tennant, D. C. (2005). *Phys. Chem. Miner.* **32**, 493–503.

Ederer, C. & Spaldin, N. A. (2006). *Curr. Opin. Solid State Mater. Sci.* **9**, 128–139.

Fiebig, M. (2005). *J. Phys. D Appl. Phys.* **38**, R123–R152.

Fischer, P., Połomska, M., Sosnowska, I. & Szymański, M. (1980). *J. Phys. C* **13**, 1931–1940.

Fruth, V., Berger, D., Matei, C., Ianulescu, A., Popa, M., Tenea, E. & Zaharescu, M. (2005). *J. Phys. IV*, **128**, 7–11.

Haumont, R., Kreisel, J., Bouvier, P. & Hippert, F. (2005). arXiv:cond-Mater/0507291.

Haumont, R., Kreisel, J., Bouvier, P. & Hippert, F. (2006). *Phys. Rev. B*, **73**, 132101.

Hill, N. A. (2000). *J. Phys. Chem. B*, **104**, 6694–6709.

Kadomtseva, A. M., Zvezdin, A. K., Popov, Yu. F., Pyatyakov, A. P. & Vorobiev, G. P. (2004). *JETP Lett.* **79**, 571–581.

Kim, J. K., Kim, S. S. & Kim, W.-J. (2005). *Mater. Lett.* **59**, 4006–4009.

Kozheev, D. F., Zalessky, A. V., Gippius, A. A., Morozova, E. N. & Bush, A. A. (2003). *Physica B*, **329**, 848–849.

Kubel, F. & Schmid, H. (1990). *Acta Cryst.* B**46**, 698–702.

Mahesh Kumar, M., Palkar, V. R., Srinivas, K. & Suryanarayana, S. V. (2000). *Appl. Phys. Lett.* **76**, 2764–2766.

Mazumder, R., Ghosh, S., Mondal, P., Bhattacharya, D., Dasgupta, S., Das, N., Sen, A., Tyagi, A. K., Sivakumar, M., Takami, T. & Ikuta, H. (2006). *J. Appl. Phys.* **100**, 033908.

Megaw, H. D. & Darlington, C. N. W. (1975). *Acta Cryst.* A**31**, 161–173.

Michel, C., Moreau, J. M., Achenbach, G. D., Gerson, R. & James, W. J. (1969). *Solid State Commun.* **7**, 701–704.

Murashov, A., Rakov, D. N., Dubienko, I. S., Zvezdin, A. K. & Ionov, V. M. (1991) *Sov. Phys. Crystallogr.* **35**, 538–541.

Niizeki, N. & Wachi, M. (1968). *Z. Kristallogr.* **127**, 173–187.

Palewicz, A., Szumiata, T., Przeniosło, R., Sosnowska, I. & Margiolaki, I. (2006). *Solid State Commun.* **140**, 359–363.

Poghossian, A. S., Abovian, H. V., Avakian, P. B., Mkrtchian, S. H. & Haroutunian, V. M. (1991). *Sens. Actuators B Chem.* **4**, 545–549.

Pradhan, A. K., Zhang, K., Hunter, D., Dadson, J. B., Loutts, G. B., Bhattacharya, P., Katiyar, R., Zhang, J., Sellmyer, D. J., Roy, U. N., Cui, Y. & Burger, A. (2005). *J. Appl. Phys.* **97**, 093903.

Przeniosło, R., Palewicz, A., Regulski, M., Sosnowska, I., Ibberson, R. M. & Knight, K. S. (2006). *J. Phys. Condens. Matter*, **18**, 2069–2075.

Przeniosło, R., Regulski, M. & Sosnowska, I. (2006). *J. Phys. Soc. Jpn*, **75**, 084718.

Rodríguez-Carvajal, J. (1993). *Physica B*, **192**, 55–69.

Ruette, B., Zvyagin, S., Pyatakov, A. P., Bush, A., Li, J. F., Belotelov, V. I., Zvezdin, A. K. & Viehland, D. (2004). *Phys. Rev. B*, **69**, 064114.

Schefer, J., Schwarzenbach, D., Fischer, P., Koetzle, Th., Larsen, F. K., Haussül, S., Rüdlinger, M., McIntyre, G., Birkedal, H. & Bürgi, H.-B. (1998). *Acta Cryst.* B**54**, 121–128.

Shaldin, Yu. V. & Matyyasik, S. (2006). *Dokl. Phys.* **51**, 397–399.

Shamir, N., Gurewitz, E. & Shaked, H. (1978). *Acta Cryst.* A**34**, 662–666.

Sosnowska, I., Loewenhaupt, M., David, W. I. F. & Ibberson, R. M. (1992). *Physica B*, **180–181**, 117–118.

Sosnowska, I., Peterlin-Neumaier, T. & Steichele, E. (1982). *J. Phys. Solid State Phys.* **15**, 4835–4845.

Sosnowska, I., Schäfer, W., Kockelmann, W., Andersen, K. H. & Troyanchuk, I. O. (2002). *Appl. Phys. A*, **74**, S1040–S1042.

Tabares-Muñoz, C., Rivera, J. P., Bezinge, A., Schmid, H. & Monnier, A. (1985). *Jpn. J. Appl. Phys.* **24**, 1051–1053.

Takahashi, K., Kida, N. & Tonouchi, M. (2006). *Phys Rev. Lett.* **96**, 117402.

Teague, J. R., Gerson, R. & James, W. J. (1970). *Solid State Commun.* **8**, 1073–1074.

Tutov, A. G. & Markin, V. N. (1970). *Izv. Akad. Nauk SSSR Neorg. Mater.* **6**, 2014–2017.

Yuan, G. L., Or, S. W., Wang, Y. P., Liu, Z. G. & Liu, J. M. (2006). *Solid State Commun.* **138**, 76–81.

Zalessky, A. V., Frolov, A. A., Khimich, T. A., Bush, A. A., Pokatilov, V. S. & Zvezdin, A. K. (2000). *Europhys. Lett.* **50**, 547–551.

Zhang, S. T., Lu, M. H., Wu, D., Chen, Y. F. & Ming, N. B. (2005). *Appl. Phys. Lett.* **87**, 262907.

Zhao, T., Scholl, A., Zavaliche, F., Lee, K., Barry, M., Doran, A., Cruz, M. P., Chu, Y. H., Ederer, C., Spaldin, N. A., Das, R. R., Kim, D. M, Baek, S. H., Eom, C. B. & Ramesh, R. (2006). *Nature Mater.* **5**, 823–829.